

RESEARCH ARTICLE

Near-Infrared Off-Axis Integrated Cavity Output Spectroscopic Dual Greenhouse Gas Sensor Based on FPGA for *in situ* Application

JIANING WANG¹, YAHUI CHUAI², PENGBO LI¹, AND GUANYU LIN¹¹Space Optics Department I, Changchun Institute of Optics, Fine Mechanics and Physics, Chinese Academy of Sciences, Changchun, Jilin 130033, China²School of Physics, Changchun University of Science and Technology, Changchun, Jilin 130022, China

Corresponding author: Guanyu Lin (linguanyu1976@163.com)

This work was supported in part by the National Natural Science Foundation of China under Grant 62005268, in part by the National Key Research and Development Program of China under Grant 2018YFB0504600 and Grant 2018YFB0504603, in part by the Science and Technology Innovation Funding for Black Land Protection under Grant XDA28050102, and in part by the State Administration of Science, Technology and Industry for National Defense Project “Research on Farultraviolet Ionospheric Imaging Technology.”

ABSTRACT In this study, we investigated the trade-off between the applicable field performance and the high sensitivity of infrared absorption sensors and provided an optimization scheme. A near-infrared greenhouse gas sensor was developed based on off-axis integrated cavity output spectroscopy (OA-ICOS) for optimal detection performance with a highly integrated design. The developed sensor included a 12 cm compact cavity length with an effective absorption path length of ~ 68.2 m, simultaneously focused on carbon dioxide (CO_2) and methane (CH_4) detection. Different from in-lab studies, the whole driving and signal processing functions were realized by a single FPGA processor. Using a calibration experiment with limited hardware resources, the developed optimized locked-in amplifier and denoising scheme improved the precision levels by ~ 3.2 times compared to a traditional design. An Allan deviation analysis showed that the minimum detection limits were optimized to 0.9 ppmv (CH_4) and 21 ppmv (CO_2). A field application was carried out in the town of SheLin over the course of 1 day, and the measurement results conformed to the gas diffusion, biological photosynthesis and respiration characteristics, which indicated the potential of the sensor for *in situ* applications. This work reveals the relationship between limited hardware resources and detection performance and provides an optimization scheme to exploit compact OA-ICOS sensors with improved sensitivity.


INDEX TERMS Off-axis integrated cavity output spectroscopy, gas sensor, near-infrared, dew condensation, greenhouse gases.

I. INTRODUCTION

Energy consumption caused by human activity has led to continuous growth in greenhouse gas emissions. Carbon dioxide (CO_2) and methane (CH_4) are identified as controlled emission gases in the Kyoto Protocol and make the most prominent contributions to greenhouse effects. CO_2 is the most significant anthropogenic greenhouse gas because of its high concentration. CH_4 has a more serious potential to cause global warming effects than CO_2 and plays a vital role in

atmospheric cycles and reactions [1]. Hence, a compact, real-time, and *in situ* monitoring sensor system to determine both CH_4 and CO_2 concentrations is urgently needed to analyze the quality of the atmospheric environment.

Commercial greenhouse gas sensors based on nondispersive near-infrared (NDIR) detection technology have advantages compared to other kinds of sensors, such as semiconductors and electrochemical sensors. Popular sensors based on NDIR technology, such as K30 (Senseair Company) and S300 (ELT Sensor Company) [2], are inexpensive and have a simpler optical structure, but they do not generate satisfying measurements. In contrast, Picarro greenhouse gas sensors, based on

The associate editor coordinating the review of this manuscript and approving it for publication was Mira Naftaly .

cavity ring-down spectroscopy (CRDS), have shown good ppb level measurement performance [3], [4]. However, this level of detection performance is superfluous for gas concentration detection in the atmosphere. Additionally, the price of a single sensor without tax is hundreds of thousands of dollars.

The basic requirements for chemical gas-phase analysis are selectivity, sensitivity and stability [5]. In theory, laser spectroscopy techniques can meet the above requirements perfectly. However, in actual implementation, there is a trade-off among the performance indicators, such as response time, long-term monitoring stability, instrument complexity and portability. Additionally, the sensitivity of a sensor based on laser spectroscopy techniques is proportional to its effective optical path length. Traditional multi-pass gas cell (MPGC) sensors are a conventional design that can achieve dozens to a few hundred meters of path length [6], [7], [8]. The main constraints for limiting path length are the mirror size and input beam quality. Compared to MPGC, integrated cavity output spectroscopy using an integral cavity with a coaxial structure such as a gas cell can easily achieve a path length that is several kilometers long [9], [10], [11]. In addition, off-axis cavity output spectroscopy (OA-ICOS) can achieve a satisfying detection performance, including high detection precision, a fast response, and insensitive to mechanical structural stability.

Based on the current reports on trace gas monitoring based on OA-ICOS, a typical molecule sensitivity range in the mid-infrared region is a popular choice to achieve high detection precision because of its strong absorption lines [12], [13]. Additionally, a commercial data acquisition card (DAQ), such as USB-62xx produced by NI, with digital signal processing based on PC is the most preferred option for providing high detection precision at the cost of a large amount hardware resources, large size, and lower cost performance [14], [15]. Therefore, a self-developed in situ trace gas detection system in the near-infrared range with a portable signal processing hardware design is still a challenge due to the trade-off between the detection precision and the applicability of in situ monitoring. In addition, besides the cavity-mode noise [16], noise that is introduced by the application environment, including mechanical vibration noise and unexpected man-made noise greatly increases the difficulty of the signal processing design.

In this article, we reported a near-infrared CH₄ and CO₂ sensor based on OA-ICOS used for real-time, in situ ambient monitoring. A small cage-based gas cell with an active pumping structure is used to reduce the response time. Additionally, an optimized digital locked-in amplifier based on FPGA is designed to realize compact and low-cost hardware implementation. The processed data are filtered by Kalman filtering (KF) to increase the signal-to-noise ratio (SNR). For field monitoring application, CH₄ and CO₂ were monitored simultaneously, and the system's detection performance was recorded effectively, including its low limitations, robustness, and reliability.

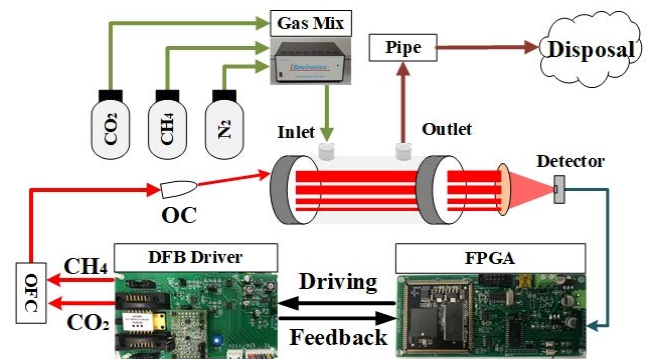


FIGURE 1. The schematic of proposed dual-gas detection system.

II. MATERIALS AND METHODS

A. SENSOR SCHEME

A self-developed CH₄ and CO₂ dual-gas sensor-based OA-ICOS was designed and implemented, and the structure of that sensor is shown in Fig.1(a). Two butterfly packaged 14-pin distributed feedback (DFB) lasers were driven and modulated to scan at around 1653.7 nm and 1573 nm, respectively, using the time-division multiplexing method (TDM). Before coupling into the integrated cavity, two emitting beams with a power of ~8 mW were combined using an optical fiber combiner (TW1650R5A1) and were collimated by an optical collimator (50-1550A-APC, Thorlabs). The high-finesse integrated cavity was nearly 10 cm long and consisted of two self-processed spherical mirrors with a reflectivity of about 99.901% at 1653.7 nm and 99.897% at 1573 nm. In order to achieve a reliable cavity that is coaxially and insensitive to temperature deformation, the cavity was designed using a cage system and fixed with an enclosure made of invar steel. The output beams from the integrated cavity were collected by a collimating lens ($f = 50\text{mm}$), and the distributed beams were converged to the photosensitive surface of near-infrared InGaAs detector. Through a sampling and impedance matching circuit, the analogous electrical signals were converged and processed by a self-developed FPGA circuit. The developed sensor including optical part and electrical part. In order to facilitate the experiments, the current gas cell has not realized the expected miniaturization. In the future improvement, the volume of optical part is able to be reduced to less than one-third of the current version. Besides the AC to DC modules, the electrical parts only contain two 12.5 cm \times 7.5 cm \times 2 cm circuit boards. The developed sensor has the further possibility to optimize the miniaturization and portability.

B. DUAL-GAS DETECTION MECHANISM

The targeted line that was selected for CH₄ absorption was the R3 branch of the two absorptions line located at 1653.7 nm and that is commonly used for CH₄ detection because of its good selectivity and strong absorption, as shown in Fig2(a). Within this wavelength range, besides the gas species with a C-H bond (C₂H₂, C₂H₄, etc.), are common interference gases

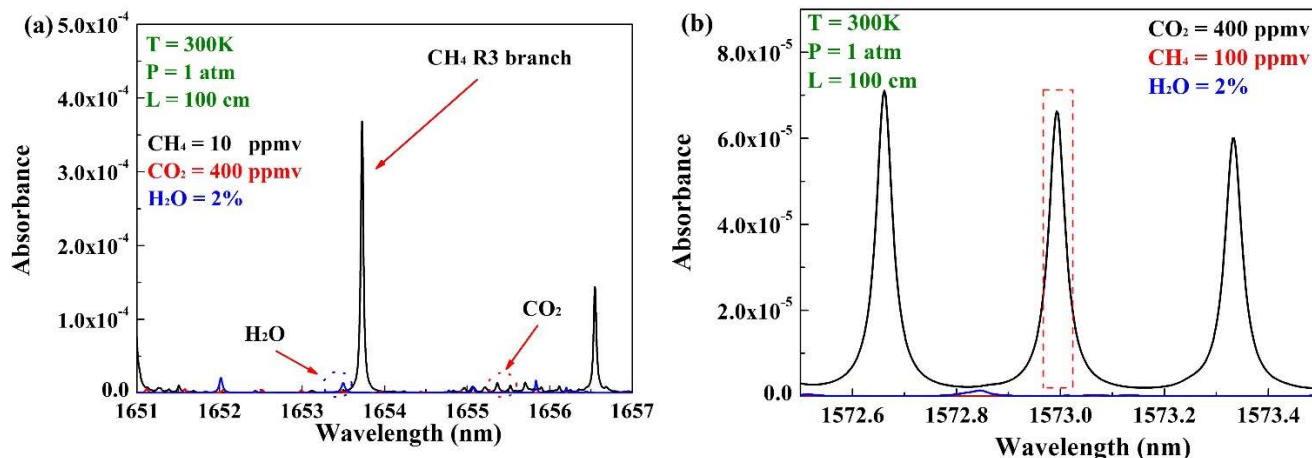


FIGURE 2. The simulated detectable absorption lines of (a) CH₄ and (b) CO₂ at room temperature and the atmospheric pressure in the region with possible interference gases.

such as CO₂ and H₂O, which are at least 3 times weaker than CH₄ and that only contribute to the background signal, and the resulting influence can be eliminated through post data processing [17]. Based on the above analysis, the error caused by the interference gas has no effect on the detection precision of CH₄ in the selected absorption range.

Considering the reflection wavelength range of spherical mirrors and the CO₂ concentration in air, the targeted line for CO₂ absorption selected was selected to be around 1573 nm, as shown in Fig2(b). Considering that the CO₂ concentration in air is ~ 400 ppmv, the targeted absorption strength of CO₂ was set to be three time lower than that of CH₄ to ensure that the concentration of the fitted curve had a satisfying resolution. The only potential interference gas around this range is H₂O, which can be ignored because of its weak absorption effect.

C. LASER CHARACTERISTIC AND MODULATION

Wavelength modulation spectroscopy (WMS) was used to improve the detection signal and noise ratio. The linewidth of both of the selected DFB lasers is nearly 2 MHz, as measured using a commercial laser linewidth measurement instrument (OE4000, OE-waves), and the output power was nearly 8 mW during the scanning period. The emission spectrum was measured using near-infrared Fourier transform (FTIR) to adjust the control temperature and current, and the results are shown in Fig 3(a) and Fig3(b). The digital PID temperature control circuit was designed with a MTD415 core chip, and the self-adjusted parameters were updated according to the RS232 ports. The dynamic fluctuations in the temperature during wavelength scanning was less than 0.005 °C.

According to previously conducted research, the modulation depth in the WMS should be 2.2 times the half width at half maximum (HEHM) of the gas absorption lines [18]. Additionally, signal processing difficulties and the frequency domain distribution of ambient noise should be comprehensively considered, so the modulation frequency was set to

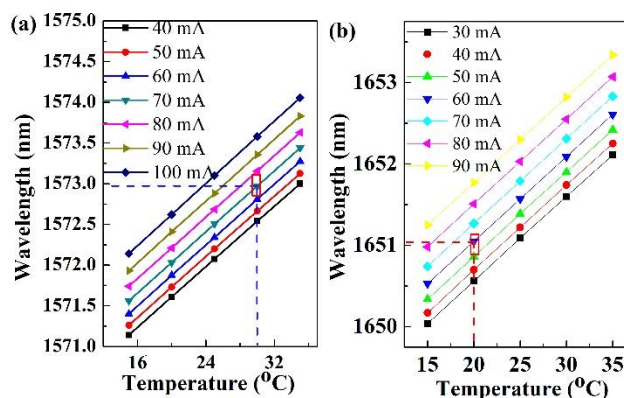


FIGURE 3. Emission spectra performance test results of (a) CO₂ and (b) CH₄ lasers for optimized driving condition selection.

1 kHz. The output 2f peak to peak amplitude of the digital signal processing mode at different modulation depths were measured at the targeted absorption lines, as shown in Fig 4. The x axis is the modulation coefficient which is the ratio of modulation depth and the half width at half maximum (HWHM). Therefore, the maximum values were achieved when the optimized modulation coefficients were 2.6(100 ppmv CO₂) and 2.8(100 ppmv CH₄), respectively.

D. EFFECTIVE PATH LENGTH DETERMINATION

During the actual implementation, it is difficult to achieve the ideal state of the OA-ICOS sensor for coupling the off-axis laser into the integrated cavity because of limitations in the lens size and light path adjustment difficulties. In our design, the cavity length is nearly 10 cm, and the reflectivity of the lens is 99.90%, while the theoretical path length is 99 m. An experimental absorption path length can be calculated according to the experimental absorption spectrum and a fitted baseline spectrum using the method reported in Ref. [19]. The measured effective light path is nearly 68.2 m, which

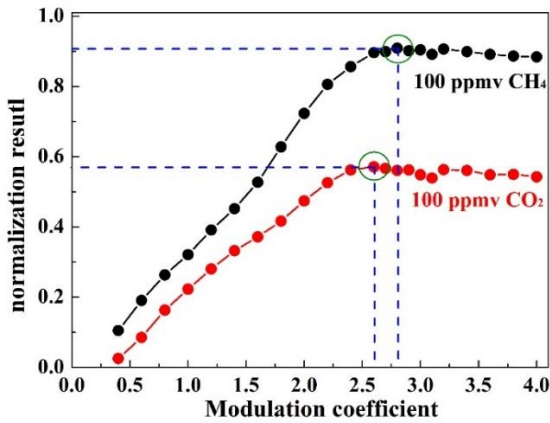


FIGURE 4. Normalized 2f amplitude versus the modulation depth for modulation depth optimization.

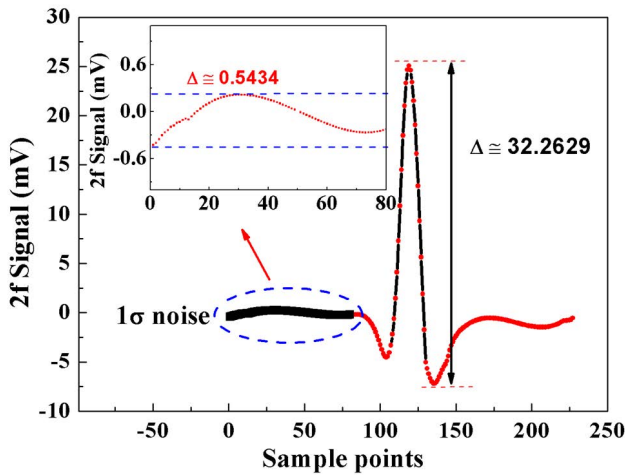


FIGURE 5. SNR evaluation using the max 2f signal and standard deviation.

implies that interference from cavity mode noise should be considered in the signal processing mode.

III. RESULTS

A. SENSING PERFORMANCE

1) GAS PREPARATION

In order to achieve accurate calibration results, the gas samples were prepared and pumped into the gas cell continuously at a certain gas flow rate. The gas samples were dynamically distributed through a mass flow meter (MT50-3G). To ensure accuracy of the results, the uncertainty of the standard gas samples was less than 2%. Different CO₂ and CH₄ samples were prepared by mixing a standard detecting gas and 99.999% N₂.

2) SNR ESTIMATION

SNR is an effective means through with to calibrate the optical path and to optimize the parameters of a system, such as the modulation depth. As shown in Fig.5, a demodulated 2f signal without any subsequent algorithm optimization was

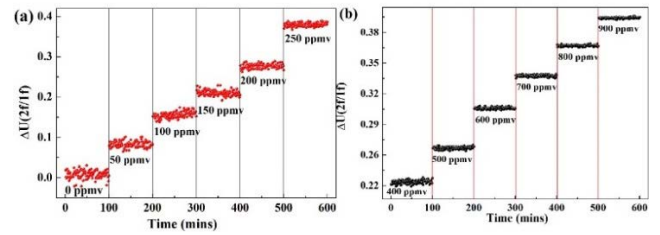


FIGURE 6. Dot plots for the extracted processed signal with different concentrations of (a) CH₄ and (b) CO₂.

obtained using a 100 ppmv CH₄ sample. The standard deviation was determined in the non-absorption range, which is about 0.5434 mV (1σ). The corresponding SNR is nearly 59.3. In the further requirements for higher detection precision, the SNR is able to be increased at the price of exhausting the of hardware’s logic resources. The asymmetrical 2f phenomenon is caused by the increasing the driving current, which can be effectively suppressed by normalizing the WMS-2f signal using the WMS-1f signal [20].

3) CALIBRATION AND DATA-FITTING

Corresponding to the ambient gas concentration, dual-gas calibration forces a different concentration range. The results determining the concentration of the detected CH₄ and CO₂ were processed and communicated using a time-sharing multiplexing method to save parallel hardware logic resource utilization. The 2f signal amplitudes of several different concentration levels were measured and are shown in Fig.6(a) and Fig.6(b), respectively, corresponding to CH₄ and CO₂. In addition, the data-fitting results demonstrate a linear response between the 2f amplitude and the concentration with an R square value of 0.9972.

The calibrated linear fitting results of CH₄ and CO₂ are shown as Eq. 1 and Eq 2.

$$C = 685.105 * \Delta U - 1.6874, \quad (1)$$

$$C = 1431.125 * \Delta U - 21.722, \quad (2)$$

The parameter C is the detecting gas concentration and ΔU is the ratio of 2f and 1f.

4) DETECTION LIMIT

The Allan deviation was used to estimate the optimal averaging time and detection limit of our detection system. In the measurements, pure dry N₂ was used to flush the gas cell for at least 10 minutes, and the long-term measurement results were recorded. The analysis results are based on Allan deviation. For the CH₄ detection shown in Fig. 7(a), the 1σ detection limit is nearly 8.9 ppmv for a 1s averaging time and the detection limit is 1.6 ppmv for a 34s optimum integral time. By comparison, the CO₂ detection precision is insufficient because of the weak absorption line. As shown in Fig. 7(b), the responding 1σ detection limit is nearly 141 ppmv for a 1s averaging time, and the detection limit is 25.6 ppmv for a 26s optimum integral time. Furthermore, the fluctuations

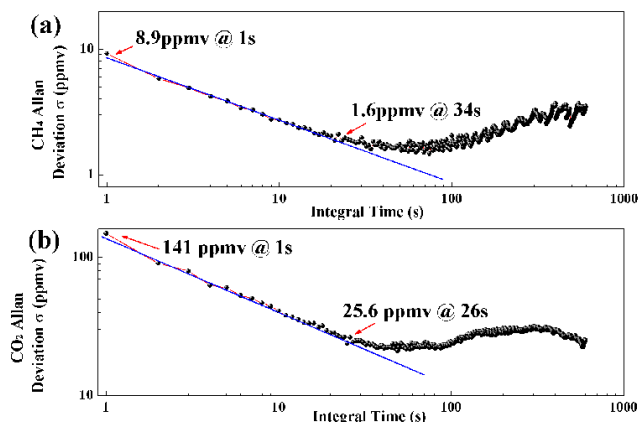


FIGURE 7. Allan deviation analysis of the sensor system based on 20 mins CH₄ and CO₂ concentration measurement results in pure N₂ atmosphere.

after the optimum integral time are mainly caused by system drifts, including ripples in the power supply, temperature fluctuations in the hardware circuits, and mechanical vibrations of the cavity during the long-term monitoring period. In addition, the detection limit performance was able to be improved based on optimized signal processing method in the following section B under the same hardware conditions.

5) RESPONSE TIME

A fast response time indicates a quasi-real time measurement and is a significant indicator in monitoring flammable and explosive materials. However, in continuous atmospheric measurement, a second level measurement delay is tolerable because of gradual changes in the characteristics of the greenhouse gas concentration. A shorter measurement period means a higher cost incurred to the limited logic resources, when the total amount of required logic resources remains unchanged in FPGA. That is to say, a fast response time occupies the resources used for high performance digital signal processing and decrease the SNR.

In order to ensure that the detection limits of both CH₄ and CO₂ are lower than the concentrations in the atmosphere, the most basic resources required for signal processing capabilities should be guaranteed. Based on the above requirements, the measurement period, including the sampling time, data preprocessing time, CIC filter delay, FIR filter delay and KT filter delay, is nearly 0.62 s. Therefore, the scan frequency is set to 1 Hz and the experimental response time is 2 s. During the experiment, the pure N₂ and 100 ppmv CH₄ samples were repeatedly injected into the cavity via mass flowmeter. In addition, according to the trialanderror method, when the response time was shortened to 0.5 s, the SNR decreased to nearly 10 dB.

B. IMPLEMENTATION OF MULTI-DENOISING SCHEMES BASED ON FPGA

Recent reports have paid more attention to detection performance, using commercial DAQ cards and PC-based signal processing, at the price of in situ application capability of

sensor and cost effects. In this design, the whole core functions, including laser driving, digital locked-in amplifier and multiple denoising schemes, such as Kalman filtering and wavelet transform, were realized based on a single FPGA chip (EP4CE40). The system clock was set to 30MHz. It is worth noting that a higher system clock input for CIC filter and FIR filter will take more logic resources implying a decrease of filtering performance. In the actual design, which has limited logic resources, the measurement precision was compared under multi-denoising schemes. In this comparison, an ~80% logic resource comprising 39600 logic elements and 116 embedded 18*18 multipliers was set as a standard resource cost to evaluate the performances of multi-denoising schemes.

1) TRADITIONAL LOCKED-IN AMPLIFIER

The locked-in amplifier method is an effective method to extract eigenfrequency signals and to suppress the noise of other frequency domains. The noise-suppress performance is proportional to the low-pass filter performance. Therefore, compared to a serial processing system such as the DSP, a parallel process chip is able to achieve a high-order filter at the price of a high resource cost. With limited resources, the cut-off frequency is lower than 10 Hz, and the filter order is 214.

2) OPTIMIZED LOCKED-IN AMPLIFIER

In order to decrease the logic utilization while ensuring filtering performance, a cascade integrator comb (CIC)filter and a lower order lower pass finite impulse response (FIR) filter are used to replace a higher order FIR. With similar filter performance to the traditional locked-in amplifier, the logic resource utilization is decreased to 62%. However, an extra delay between the CIC filter and FIR filter is about 78ms which may limit the shortest detection period. The influencing factors of this delay time includes the system clock, filter orders and sampling frequency, which are recommended to be adjusted according to specific requirements in practical applications. It is worth noting that shortening of the delay time will lead to an increase in resource consumption. In each measurement period, there is a bump caused by the sudden switching of periodic triangular wave on the beginning of the waveform. In each scanning period, the 2f peak appears in a nearly fixed time range. Therefore, the peak to peak finding processing can avoid this bump. The raw signal and processed output in each step are shown in Fig. 8.

3) WAVELET TRANSFORM SCHEME

Wavelet Transform is a suitable denoising scheme for FPGA because of the low multiplier utilization. It consists of three key parts, which are wavelet basic function, wavelet decomposition level and wavelet threshold. In this work, the basic function selected for wavelet was “Daubechies”, that was able to be used in the discrete wavelet transform. The length of the filter was set to 16. Perform 4 level wavelet decomposition processing on noisy signal. The typical Heursure

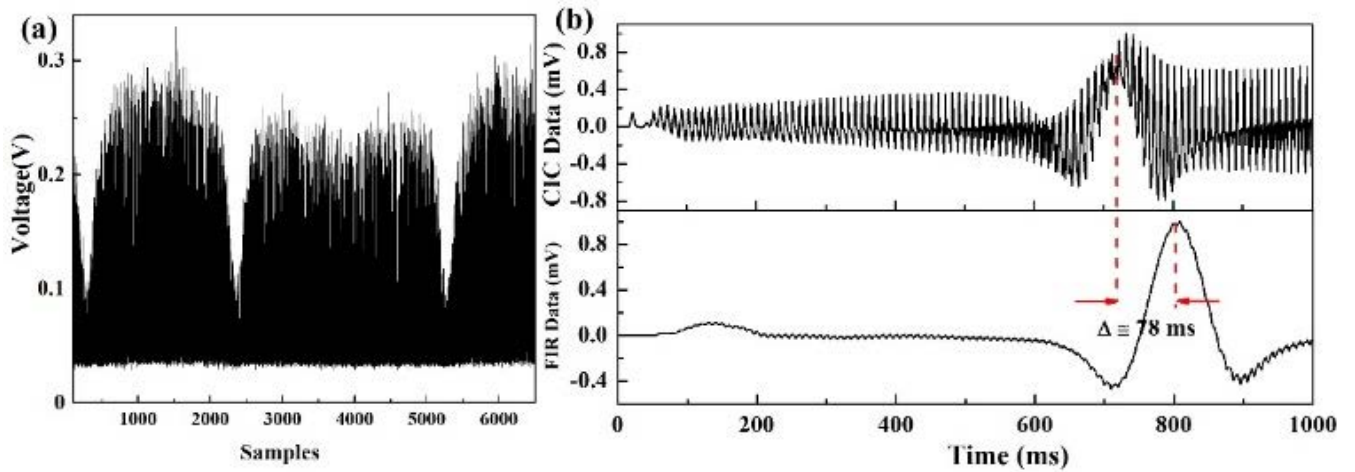


FIGURE 8. (a) The measured output detection signal of the preamplifier circuits; (b) processed 2f signal from CIC filter and FIR filter, respectively.

threshold and local threshold functions were selected to realize the optimized denoising performance. The split, predict and update processes were realized by latch, shifter, and logical judgements. The main resources occupancy is determined by the resolution bit width.

4) KALMAN FILTERING SCHEME

The Kalman filter has a satisfying suppression effect on the Gaussian noise of dynamic systems. In the prediction equation, the ratio of the state transition matrix and state observation matrix was normally adjusted according to the actual requirements of filtering performance and response seep. The filter performance increase, with a higher ratio value, at the price of long response delay. In this work, the ratio of the state transition matrix and state observation matrix was set to 200 to balance the requirement between high filtering efficiency and response delay. And the first 20 measured signals were selected as the original input. In the implementation of FPGA code, the D flip-flop and state machine are the main logic resource used to build the Kalman Filtering.

With the limited logic resource, the different denoising schemes including traditional locked-in amplifier, Wavelet transform and Kalman filtering are used to process the original 2f signals and the results are shown in Fig. 9. These denoising schemes were developed in the same hardware platform and the experimental results were acquired sequentially. The processed 2f signal were recorded over 50 minutes. Compared to traditional locked-in amplifier, both Wavelet transform scheme and Kalman filtering scheme decrease the noise level over 2.5 times.

5) COMPARISON AMONG MULTI-DENOISING SCHEMES

Using the same logic resources, the noise suppression performance using multi-denoising methods was compared. During the experiments, the baseline noise in the sensor was measured under a N2 atmosphere for half hours. The detection data were sampled from the CH4 channel as an example, and

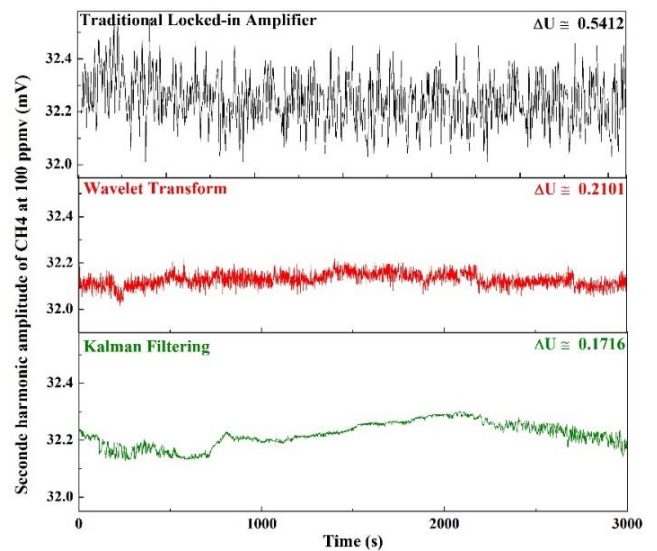


FIGURE 9. Second harmonic amplitudes fluctuation of CH4 at 100 ppmv using different denoising schemes including traditional locked-in amplifier, wavelet transform and kalman filtering.

the comparison results are shown in Table 1. In this table, the raw data processed with the traditional locked-in amplifier method were set at a standard level with a standard deviation factor of 1. The detection limits were obtained for an average time of 1 second, as calculated by Allan deviation. The extra delay in the wavelet transforms and Kalman filtering was mainly caused by the data latch and error of the divided trigger clock in discrete FPGA system. In contrast, the delay of the cascaded filters is still the main source of delay in the system. In addition, the amount of logic resources used for signal processing is about 80% of the total amount of resources.

According to the above analysis, with limited logic resources, a digital signal processing model with an optimized locked-in amplifier and Kalman filter can achieve

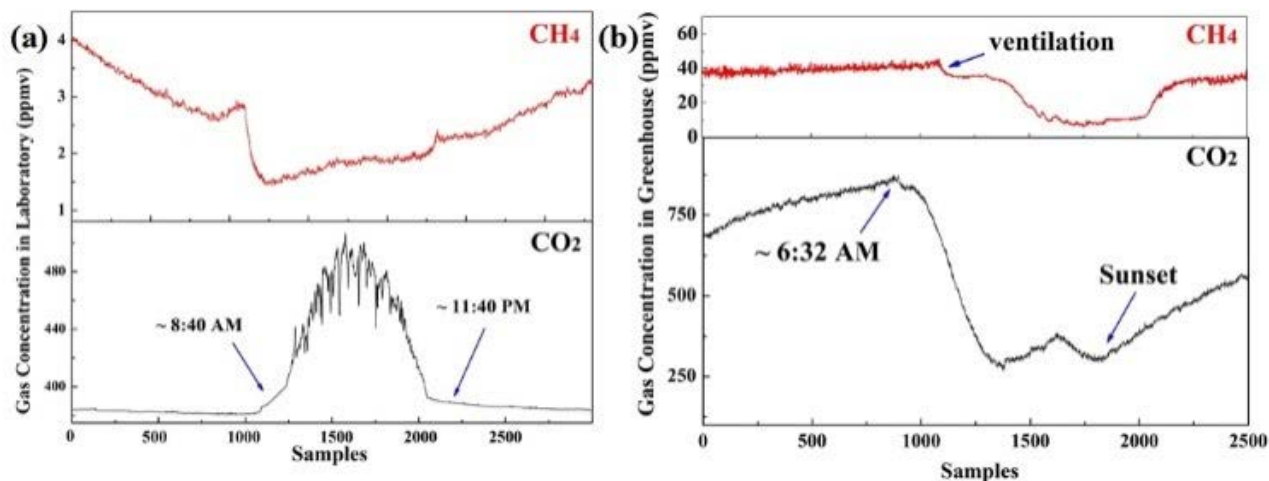


FIGURE 10. Continuous ~24 hours monitoring of CH₄ concentration and CO₂ concentration (a) in a laboratory and (b) in a greenhouse in Mar. 2022 in SheLing.

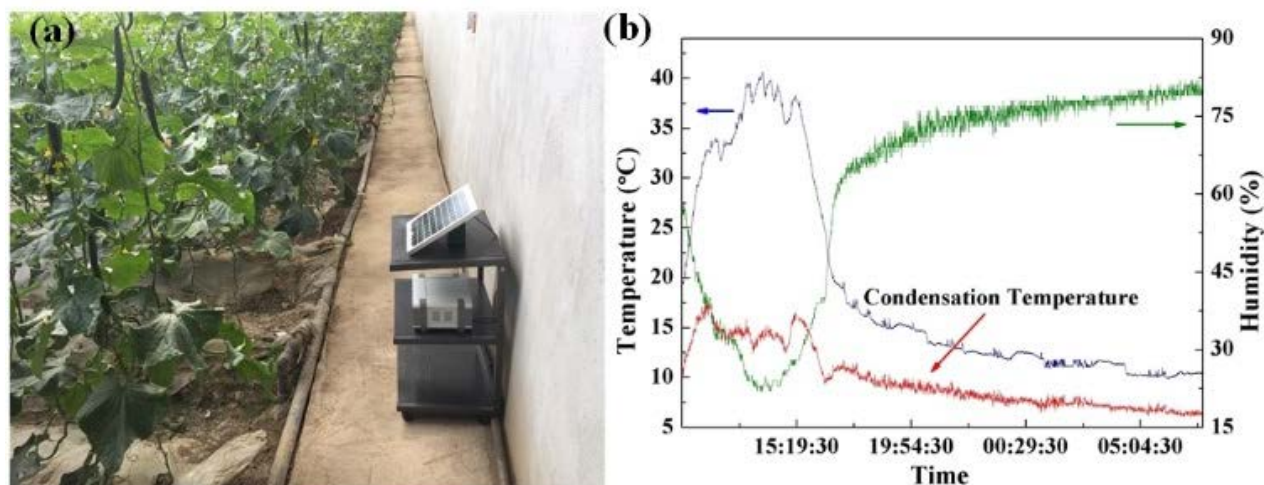


FIGURE 11. (a) The instalment of the sensor in greenhouse; (b) temperature, humidity and dew condensation results of critical optical components.

desirable detection performance. For example, the detection limit of CH₄ is improved from 8.9 ppmv to 0.9 ppmv at 1 second. Under even higher precision detection requirement, the detection limit is able to furtherly enhanced at the price of longer integration time. In the communication hardware design, critical parameters including integration time, R and Q of Kalman filtering. etc is able to be injected through RS232 to improve the applicability of the instrument to different environments.

Based on this scheme, the power consumption was recorded continuously, and the average power consumption was lower than 1.24W, which included the total power consumptions except laser drive. Therefore, the further optimization to achieve miniaturization based on the battery power supply is possible.

IV. FIELD APPLICATION

A. FIELD APPLICATION IN LAB AND GREENHOUSE

As shown in Fig. 10(a), a continual experiment was carried out in laboratory in atmospheric environment. Considering

the lower concentration of CH₄ in atmospheric, the integration time is set to 30 seconds injecting through RS232 port. The CH₄ concentration during daytime was slightly lower than that at nighttime. The most possible reason was related to boundary layer dynamics and the extent of atmospheric mixing. And the CO₂ concentration during daytime had an obvious increase with irregular fluctuation because of the human activities.

In the greenhouse environment, because of the human activities, the sudden changes of gas concentration are more common in greenhouse. Therefore, the Q parameter of KF filter is slightly increased. And the measured CH₄ concentration is much higher than the average concentration in the atmosphere. This phenomenon is caused by CH₄ production and its release from soil microorganisms, such as methanotrophs, and chemical reactions of fertilizers [21]. In contrast, the measured CO₂ concentration data mainly complied with the data for photosynthesis and artificial ventilation, implying a desired detection performance [22]. In the daytime, human activities, such as ventilation and human respiration, increase

TABLE 1. Comparison among different denoising schemes (traditional locked-in, optimized locked-in, wavelet transform and kalman filtering).

Method	Detection Limit (ppmv @ 1s)	Extra Delay (ms)	Logic Resource Distribution	Standard Deviation Factor
<i>Traditional locked-in Amplifier</i>	8.9 (CH ₄) 141 (CO ₂)	--	Multi:12% FIR:88%	1
<i>Optimized locked-in Amplifier</i>	4.2 (CH ₄) 82 (CO ₂)	<100	Multi:12% CIC:9% FIR:79%	1.68
<i>Wavelet Transform</i>	2.2 (CH ₄) 52 (CO ₂)	<120	Multi:12% CIC:9% FIR:72% WT:7%	2.6
<i>Kalman Filtering</i>	0.9 (CH ₄) 21 (CO ₂)	<120	Multi:12% CIC:9% FIR:68% KF:11%	3.2

of CO₂ concentration. In addition, the greenhouse used for the field application is a semi-enclosed structure. The higher CO₂ concentration at night is caused by the plant respiration drifting to the outside and the growth trend of the CO₂ concentration became flat as the CO₂ concentration decreased.

B. DEW CONDENSATION TEST

The risk of condensation forming on a mirror is one of the major threats to the application reliability of our sensor in complex environments, such as in a greenhouse. The sensor as installed in a greenhouse, and the results of the field experiments are shown in Fig.11(a) and Fig.11(b), respectively. Commercial temperature and humidity sensors, SHT75 (Sensirion, Laubisruetistrasse), were installed on key optical components, such as reflection mirrors. The humidity and temperature accuracy were 3.0% and 0.4 °C, respectively. During the in-situ application, potential errors were caused by measurement factors, such as the supply voltage, ADC resolution, etc., which were calibrated. The calculated dew condensation temperature is represented by a red curve and was determined using the Barenbrug formula, which has an uncertainty of 0.4 °C. At night, the safety margin between the condensation temperature and the actual temperature was less than 3 °C, which simplifies a potential condensation risk. Constant temperature control may eliminate the potential condensation but possibly at the price of more power consumption.

V. CONCLUSION

The design and implementation of a novel in situ dual greenhouse gas monitoring sensor was presented, and the reserach fully considered the miniaturization of the sensor and the applicability of in situ application. The CH₄ and CO₂ detection limits were determined to be 0.9 ppmv and 21 ppmv, respectively, satisfying the in-situ application requirements. Due to the limited logic resources, the utilization of an optimized locked-in amplifier with Kalman filtering demonstrated better signal processing performance.

The field experiments were demonstrated in a greenhouse, which further validated the stability of the sensor system for greenhouse gas monitoring in-suit. There is a potential risk of dew condensation, and this should be prevented. Further efforts will be made to determine further trade-offs and optimization possibilities to enhance detection performance, the minimum size of the sensor for integration and cost effective, and expandable applicability to other field deployment tasks, such as urban natural gas leakage inspections.

To insert images in *Word*, position the cursor at the insertion point and either use Insert | Picture | From File or copy the image to the Windows clipboard and then Edit | Paste Special | Picture (with “float over text” unchecked).

IEEE will do the final formatting of your paper. If your paper is intended for a conference, please observe the conference page limits.

REFERENCES

- [1] J. Wang, B. Li, G. Lin, Q. Ma, S. Wang, and M. Piao, “Near-infrared methane sensor based on a distributed feedback laser,” *Spectrosc. Lett.*, vol. 52, no. 2, pp. 113–120, Feb. 2019.
- [2] M. Assali and C. Fittschen, “Rate constants and branching ratios for the self-reaction of acetyl peroxy (CH₃C(O)O₂•) and its reaction with CH₃O₂,” *Atmosphere*, vol. 13, no. 2, p. 186, Jan. 2022.
- [3] H. Chen, “High-accuracy continuous airborne measurements of greenhouse gases (CO₂ and CH₄) using the cavity ring-down spectroscopy (CRDS) technique,” *Atmos. Meas. Techn.*, vol. 3, no. 2, pp. 375–386, 2010.
- [4] T. Yasuda, S. Yonemura, and A. Tani, “Comparison of the characteristics of small commercial NDIR CO₂ sensor models and development of a portable CO₂ measurement device,” *Sensors*, vol. 12, no. 3, pp. 3641–3655, Mar. 2012.
- [5] C. Zheng, T. Ye, W. L. Sanchez, N. P. C. Li, Lei, D. Wang, Y. Griffin, and R. J. Tittel, “Development and field deployment of a mid-infrared methane sensor without pressure control using interband cascade laser absorption spectroscopy,” *Sensors Actuators B, Chem.*, vol. 244, pp. 365–372, Jun. 2017.
- [6] J. Shemshad, S. M. Aminossadati, and M. S. Kizil, “A review of developments in near infrared methane detection based on tunable diode laser,” *Sens. Actuators B, Chem.*, vols. 171–172, pp. 77–92, Aug/Sep. 2012.
- [7] K. Liu, L. Wang, T. Tan, G. Wang, W. Zhang, W. Chen, and X. Gao, “Highly sensitive detection of methane by near-infrared laser absorption spectroscopy using a compact dense-pattern multipass cell,” *Sens. Actuators B, Chem.*, vol. 220, pp. 1000–1005, Dec. 2015.
- [8] W. Ren, L. Luo, and F. K. Tittel, “Sensitive detection of formaldehyde using an interband cascade laser near 3.6 μm,” *Sens. Actuators B, Chem.*, vol. 221, pp. 1062–1068, Dec. 2015.
- [9] G. Zhao, T. Hausmaninger, W. G. Ma, and O. Axner, “Shot-noise-limited Doppler-broadened noise-immune cavity-enhanced optical heterodyne molecular spectrometry,” *Opt. Lett.*, vol. 43, no. 4, pp. 715–718, 2018.
- [10] K. Zheng, C. Zheng, N. Ma, Z. Liu, Y. Yang, Y. Zhang, Y. Wang, and F. K. Tittel, “Near-infrared broadband cavity-enhanced spectroscopic multigas sensor using a 1650 nm light emitting diode,” *ACS Sensors*, vol. 4, no. 7, pp. 1899–1908, Jul. 2019.
- [11] W. Ren, Z. Wang, Q. Wang, W. P. Zhang, and H. Y. Wei, “Ultra-sensitive photoacoustic detection in a high-finesse cavity with Pound-Drever–Hall locking,” *Opt. Lett.*, vol. 44, no. 8, pp. 1924–1927, 2014.
- [12] K. Y. Zheng, “Near-infrared acetylene sensor system using off-axis integrated-cavity output spectroscopy and two measurement schemes,” *Opt. Exp.*, vol. 26, no. 20, pp. 26205–26216, Oct. 2018.
- [13] C. Zellweger, L. Emmenegger, M. Firdaus, J. Hatakka, M. Heimann, E. Kozlova, T. G. Spain, M. Steinbacher, M. V. van der Schoot, and B. Buchmann, “Assessment of recent advances in measurement techniques for atmospheric carbon dioxide and methane observations,” *Atmos. Meas. Techn.*, vol. 9, no. 9, pp. 4737–4757, Sep. 2016.

[14] K. Y. Zheng, C. T. Zheng, H. P. Zhang, J. H. Li, Z. D. Liu, Z. Y. Chang, Y. Zhang, Y. D. Wang, and F. K. Tittel, "Near-infrared off-axis integrated cavity output spectroscopic gas sensor for real-time, *in situ* atmospheric methane monitoring," *IEEE Sensors J.*, vol. 21, no. 5, pp. 6830–6838, Mar. 2021.

[15] K. Zheng, C. Zheng, J. Li, N. Ma, Z. Liu, Y. Li, Y. Zhang, Y. Wang, and F. K. Tittel, "Novel gas-phase sensing scheme using fiber-coupled off-axis integrated cavity output spectroscopy (FC-OA-ICOS) and cavity-reflected wavelength modulation spectroscopy (CR-WMS)," *Talanta*, vol. 213, Jun. 2020, Art. no. 120841.

[16] J. J. Wang, X. Tian, Y. J. Dong, J. Chen, T. Tan, G. D. Zhu, W. D. Chen, and X. M. Gao, "High-sensitivity off-axis integrated cavity output spectroscopy implementing wavelength modulation and white noise perturbation," *Opt. Lett.*, vol. 44, no. 13, pp. 3298–3301, Jul. 2019.

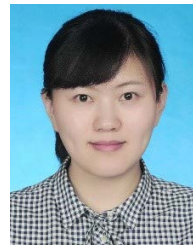
[17] C. Zheng, W. Ye, N. P. Sanchez, A. K. Gluszek, A. J. Hudzikowski, C. Li, L. Dong, R. J. Griffin, and F. K. Tittel, "Infrared dual-gas CH₄/C₂H₆ sensor using two continuous-wave interband cascade lasers," *IEEE Photon. Technol. Lett.*, vol. 28, no. 21, pp. 2351–2354, Nov. 1, 2016.

[18] C. Shi, D. Wang, Z. Wang, L. H. Ma, Q. Wang, K. Xu, S. C. Chen, and W. Ren, "A mid-infrared fiber-coupled QEPAS nitric oxide sensor for real-time engine exhaust monitoring," *IEEE Sensors J.*, vol. 17, no. 22, pp. 7418–7424, Oct. 2017.

[19] M. Donget, C. T. Zheng, D. Yao, G. Q. Zhong, S. Z. Miao, W. L. Ye, Y. D. Wang, and F. K. Tittel, "Double-range near-infrared acetylene detection using a dual spot-ring Herriott cell (DSR-HC)," *Opt. Exp.*, vol. 26, no. 9, pp. 12081–12091, Apr. 2018.

[20] C. Li, L. Dong, C. Zheng, and F. K. Tittel, "Compact TDLAS based optical sensor for ppb-level ethane detection by use of a 3.34 μm room-temperature CW interband cascade laser," *Sens. Actuators B, Chem.*, vol. 232, pp. 188–194, Sep. 2016.

[21] X. Liu, L.-D. Shen, W.-T. Yang, M.-H. Tian, J.-H. Jin, Y.-L. Yang, J.-Q. Liu, Z.-H. Hu, and H.-S. Wu, "Effect of elevated atmospheric CO₂ concentration on the activity, abundance and community composition of aerobic methanotrophs in paddy soils," *Appl. Soil Ecol.*, vol. 170, Feb. 2022, Art. no. 104301.



YAHUI CHUAI received the Ph.D. degree from Jilin University, Changchun, China, in 2016. Since 2016, she has been a Teacher at the Institute of Physics, Changchun University of Science and Technology. Her research interests include the visible light-infrared transparent conductive film, semiconductor optoelectronic device, and oxide semiconductor material sensor.



PENGBO LI was born in Pingdingshan, Henan, China, in 1998. He received the B.S. degree in vehicle engineering from the Southwest Jiaotong University, in 2020. He will pursue the M.S. degree in mechanical engineering with the Changchun Institute of Optics, Fine Mechanics and Physics, University of Chinese Academy of Sciences.



GUANYU LIN was born in Changchun, Jilin, China, in 1976. He received the B.S. and M.S. degrees in mechanical engineering from the Jilin University of Technology and Jilin University, in 1998 and 2003, respectively, and the Ph.D. degree in mechanical engineering from the University of Chinese Academy of Sciences, in 2007.



JIANING WANG received the B.Eng. degree from the School of Opto-Electronic Engineering, Changchun University of Science and Technology, in 2010, the M.Sc. degree in electrical engineering from the University of Melbourne, in 2013, and the Ph.D. degree in circuit and system from Jilin University, in 2017.

He joined the Space Optics Department I, Changchun Institute of Optics, Fine Mechanics and Physics (CIOMP), as an Assistant Professor, in 2017, and participates in the development of FengYun series meteorological satellites. His research interests include infrared absorption spectroscopy, signal processing based on PFGA, and optical gas sensors.

From 2007 to 2010, he was an Assistant Professor with the Changchun Institute of Optics, Fine Mechanics and Physics, Chinese Academy of Sciences. Since 2015, he has been a Professor with the Mechanical Automation Department. He is the first author of more than 30 articles and more than 20 inventions. His research interests include satellite payload development and ultraviolet optical remote sensing research and design of spectral analysis instrument for atmospheric detection.

Dr. Lin was a recipient of the Second Prize of National Science and Technology Progress Award (Chinese National Level Award), in 2019, and the First Prize of Space Gas Detection Technology (Provincial Level), in 2012.

...